Journal of Catalysis **185,** 252–264 (1999)
Article ID jcat.1999.2517, available online at http://www.idealibrary.com on IDEAL®

Active Oxygen Species and Mechanism for Low-Temperature CO Oxidation Reaction on a TiO_2-Supported Au Catalyst Prepared from $Au(PPh_3)(NO_3)$ and As-Precipitated Titanium Hydroxide

Haichao Liu,* Alexander I. Kozlov,* Anguelina P. Kozlova,* Takafumi Shido,* Kiyotaka Asakura,† and Yasuhiro Iwasawa*,[1]

*Department of Chemistry, Graduate School of Science, The University of Tokyo, Hongo, Bunkyo-ku, Tokyo 113-0033, Japan; and †Research Center for Spectrochemistry, Graduate School of Science, The University of Tokyo, Hongo, Bunkyo-ku, Tokyo 113-0033, Japan

Received November 17, 1998; revised April 7, 1999; accepted April 8, 1999

The active oxygen species and mechanism for catalytic CO oxidation with O_2 on a highly active TiO_2-supported Au catalyst (denoted as Au/Ti(OH)$_4^*$), which was prepared by supporting a Au–phophine complex on as-precipitated wet titanium hydroxide followed by calcination at 673 K, have been studied by means of oxygen isotope exchange, O_2 temperature-programmed desorption (O_2 TPD), electron spin resonance (ESR), and Fourier-transformed infrared spectroscopy (FT-IR). Surface lattice oxygen atoms on the Au/Ti(OH)$_4^*$ catalyst were inactive for oxygen exchange with O_2 and CO and also for CO oxidation at room temperature. The surface lattice oxygen atoms were exchanged only with the oxygen atoms of CO_2, probably via carbonates. O_2 did not dissociate to atomic oxygen on the catalyst. The catalyst showed a paramagnetic signal at $g = 2.002$ due to unpaired electrons trapped at oxygen vacancies mainly at the surface. O_2 adsorbed on the oxygen vacancies to form superoxide O_2^- with $g_1 = 2.020$, $g_2 = 2.010$, and $g_3 = 2.005$, which are characteristic of O_2^- with an angular arrangement. Upon CO exposure, all the adsorbed oxygen species disappeared. The adsorbed oxygen on Au/Ti(OH)$_4^*$ desorbed below 550 K. O_2^- species were also observed on TiO$_2^*$ prepared by calcination of as-precipitated wet titanium hydroxide at 673 K, but were unreactive with CO. FT-IR spectra revealed that CO reversibly adsorbed on both Au particles and Ti^{4+} sites on the Au/Ti(OH)$_4^*$ surface. No band for adsorbed CO was observed on the TiO$_2^*$, which indicates that the presence of Au particles has a profound effect on the surface state of Ti oxide. No shifts of ν_{CO} peaks on Au/Ti(OH)$_4^*$ occurred upon O_2 adsorption, suggesting that O_2 was not directly bound to the Au particles on which CO adsorbed. Annealing of Au/Ti(OH)$_4^*$ under O_2 atmosphere significantly suppressed the O_2 adsorption and the CO oxidation due to a decrease in the amount of oxygen vacancies, while CO adsorption was not affected by annealing. From the systematic oxygen isotope exchange experiments along with O_2-TPD, ESR, and FT-IR, it is most likely that CO adsorbed on Au metallic particles and O_2^- adsorbed on oxygen vacancies at the oxide surface adjacent to the Au particles contribute to the low-temperature catalytic CO oxidation. The mechanism for the catalytic CO oxidation on the active Au/Ti(OH)$_4^*$ catalyst is discussed in detail and compared with mechanisms reported previously.

Key Words: **active oxygen species; mechanism; CO oxidation; oxygen isotope exchange; Au catalyst; catalyst preparation; ESR; TPD; FT-IR.**

1. INTRODUCTION

While gold has been demonstrated to be chemically most inactive among noble metals due to its electronic configuration (1), matrix-trapped Au atoms are known to be reactive for CO oxidation even at 30–40 K (2). The renewal in interest in Au catalysis following Huber *et al.*'s (2) report was spurred by Haruta *et al.*'s (3) finding of high catalytic performance of dispersed Au particles, prepared by coprecipitation and deposition–precipitation, in low-temperature CO oxidation. Gold metal finely dispersed on metal oxides has been demonstrated to be a promising catalyst in a number of catalytic reactions including complete oxidation of hydrocarbons, hydrogenation, water–gas shift reaction, and NO reduction (4–14). Moreover, supported Au catalysts are also promising catalysts in various practical areas such as CO removal in CO_2 lasers, CO gas sensors, air-purification devices for respiratory protection, and pollution control devices for removing trace quantities of CO from ambient air in submarines and space crafts on long missions (5–7). Three methods, coprecipitation, deposition–precipitation, and chemical vapor deposition, have been employed to prepare highly dispersed Au catalysts (4, 5).

We have developed a new way to obtain dispersed Au particles on oxide surfaces (11–14). The key issues for preparation are: (i) choice of suitable Au complexes as precursors for Au particles, (ii) use of as-precipitated wet metal hydroxides as precursors for oxide supports, which have many surface OH groups reactive to the Au complexes, and (iii) simultaneous transformation of both precursors

[1] To whom correspondence should be addressed. Fax: 81-3-5800-6892. E-mail: iwasawa@chem.s.u-tokyo.ac.jp.

0021-9517/99 $30.00

to gold particles and oxides under their chemical interactions by temperature-programmed calcination (13, 14). We found that Au–phosphine complexes are good candidates for metal precursors because Au–phosphine complexes are thermally decomposed to Au metal in a temperature range similar to that used for the transformation of wet metal hydroxides to oxides, and the phosphine ligands are expected to retard the growth to large Au metallic particles (11–14). The steady-state rate of CO oxidation on an Fe oxide-supported 0.5 wt% Au catalyst prepared from Au(PPh_3)(NO_3) and as-precipitated wet iron hydroxide was 3.9×10^{-2} mol CO/mol Au/s at 252 K. The rate was higher than that of the corresponding coprecipitated catalysts calcined under the identical conditions by a factor of >3. Activities of conventional impregnation catalysts were lower by at least two orders of magnitude. Highly active catalysts were also obtained when [$Au_9(PPh_3)_8(NO_3)_3$] (12) and Au(NO_3)($CNBu^t$) (15) were used as precursors. In the case of titania-supported Au catalysts the new preparation method gave a Ti oxide-supported Au catalyst with an activity of 9.6×10^{-3} mol CO/mol Au/s at 300 K (12, 16). Similar activity (1×10^{-2} mol CO/mol Au/s at 315 K) was also observed for a catalyst prepared by CVD of Me_2Au(acac) on anatase powder (17).

It is now documented that the activity of gold catalysts for CO oxidation is sensitive to the nature of support, the size of gold particles, and the properties of the gold–support interface. The low melting point of gold results in difficulty preparing gold catalysts in a highly dispersed state. The possibility of fast Au agglomeration during catalyst preparation may be one of the main reasons why choice of a preparation method has profound effects on the catalytic activity of gold-containing materials to a much greater extent than in the cases of other noble metal catalysts. Factors that determine the catalytic activity of supported gold catalysts prepared by coprecipitation and deposition–precipitation methods (4, 5, 18–20) have been studied by several groups (4–10, 18), and factors that affect performance of the newly developed Au catalysts have been discussed by us (12–14, 16).

As for the mechanism for CO oxidation on the active Au catalysts, the active oxygen species and the role of lattice oxygen atoms have not been clarified. There still exists controversy as to whether molecular oxygen or atomic oxygen contributes to CO oxidation. To explain the high activity of coprecipitated and deposition–precipitated Au catalysts, a scheme that involves catalysis at the boundary of small Au particles and oxide support was proposed by Haruta *et al.* (4, 5, 21). The proposed mechanism involves reversible adsorption of CO on the surface and perimeter of Au particles and irreversible adsorption of oxygen at the boundary to form a OC–Au–O intermediate via oxygen dissociation, followed by CO_2 formation at the boundary. Boccuzzi *et al.* (22, 23) claimed that adsorption of oxygen changed CO stretching frequencies, which may indicate the adsorption of CO and oxygen in the neighborhood of each other on a gold particle, supporting the formation of OC–Au–O species. Further, the formation of atomic oxygen species on deposition–precipitated Au/TiO_2 and coprecipitated Au/ZnO was also suggested by noticeable oxygen scrambling in the reaction of $C^{16}O + {}^{36}O_2$ (22). The existence of another independent, slower pathway involving oxygen atoms of the oxide supports was also demonstrated (22). Knell *et al.* (24) claimed that CO oxidation on the coprecipitated Au/ZrO_2 catalyst involves interaction of CO with surface OH groups to form surface formates that can be oxidized by atomic oxygen activated on the surface of Au metallic particles, though such a route was excluded on Au/TiO_2 and Au/ZnO pretreated in dry air (22). In contrast to these results, the temperature-programmed desorption measurements following the adsorption of a mixture of ${}^{32}O_2$ and ${}^{36}O_2$ on the active Au catalysts prepared using the Au–phosphine precursors and the as-precipitated wet metal hydroxide precursor exhibited a single desorption peak of ${}^{32}O_2$ or ${}^{36}O_2$. No ${}^{16}O^{18}O$ was observed, suggesting the absence of active atomic oxygen species and no exchange between ${}^{32}O_2$ and ${}^{36}O_2$ nor between ${}^{36}O_2$ and lattice ${}^{16}O$ atoms. Further, in the reaction $C^{16}O + {}^{36}O_2$, neither ${}^{16}O^{18}O$ nor $C^{18}O$ was detected. The results on the newly developed Au catalysts were entirely different from those reported on the deposition–precipitated Au/TiO_2 and coprecipitated Au/ZnO catalysts.

Thus, these conflicting results tempted us to examine the reaction mechanism for CO oxidation on the active Au catalyst prepared from Au(PPh_3)(NO_3) and as-precipitated wet metal hydroxide precursors. Elucidation of the reaction mechanism and active oxygen species may be relevant to development of new oxidation catalysts. In the present paper we report a systematic study of the Ti oxide-supported Au catalyst using oxygen isotope exchange, Fourier-transformed infrared spectroscopy (FT-IR), electron spin resonance (ESR), and temperature-programmed desorption (TPD).

2. EXPERIMENTAL

Catalyst Preparation

Supported gold catalysts were prepared by using Au(PPh_3)(NO_3) and as-precipitated wet titanium hydroxide in the same manner as that described in the previous reports (11–13). As-precipitated titanium hydroxide Ti(OH)$_4^*$ was obtained by hydrolysis of Ti($O^iC_3H_7$)$_4$ (99.999% purity) with an aqueous NH_3 solution. The precipitate was then filtrated and washed with deionized water until the pH value became 7.0. The as-prepared wet Ti(OH)$_4^*$ was impregnated with an acetone solution of Au(PPh_3)(NO_3) under vigorous stirring, followed by vacuum drying to

remove the solvent at room temperature. The obtained sample was heated to 673 K at a ramping rate of 4 K min^{-1} and kept at this temperature for 4 h in a flow of air (30 ml/min). The catalyst thus obtained is denoted as Au/$Ti(OH)_4^*$. Tianium oxide in the Au/$Ti(OH)_4^*$ catalyst was amorphous according to the XRD pattern (12, 16). The Au loading used in this work was 3 wt%. For comparison, amorphous TiO_2^* was obtained by calcination of the as-precipitated wet $Ti(OH)_4^*$ in a similar way. The BET surface areas for TiO_2^* and Au/$Ti(OH)_4^*$ were 86 and 82 $m^2 g^{-1}$, respectively.

Oxygen Isotope Exchange and CO Oxidation

Oxygen isotope exchange reactions were carried out in a closed circulating system (dead volume, 134 cm^3) equipped with a quadruple mass spectrometer (AQA-100R). Before each reaction Au/$Ti(OH)_4^*$ or TiO_2^* was pretreated with 13.3 kPa of $^{32}O_2$ at 673 K for 1 h, followed by evacuation at 673 K for 1 h. After cooling to room temperature under vacuum, 0.67 kPa of $^{36}O_2$ (99.2% purity) or an equimolar mixture of $^{32}O_2 + {}^{36}O_2$ (0.67 kPa of each) was introduced into the system. The oxygen isotopomers $^{32}O_2$ ($^{16}O^{16}O$), $^{34}O_2$ ($^{16}O^{18}O$), and $^{36}O_2$ ($^{18}O^{18}O$) were analyzed using a quadruple mass spectrometer. CO oxidation reaction was also induced in the same closed circulating system after the introduction of an equimolar mixture $^{32}O_2 + C^{16}O$ or $^{36}O_2 + C^{16}O$ (0.67 kPa for each).

To study an annealing effect of Au/$Ti(OH)_4^*$ after calcination, the CO oxidation reaction was also induced on the Au/$Ti(OH)_4^*$ sample pretreated with 13.3 kPa of O_2 at 673 K for 1 h, followed by cooling to 298 K under the ambient O_2 and evacuation at 298 K for 1 h (denoted as annealed Au/$Ti(OH)_4^*$ hereinafter).

Kinetics of CO Oxidation

Kinetic measurements were carried out in a glass fixed-bed flow reactor operating in a differential mode. The conversions of CO and O_2 were kept below 15%. The reactants were diluted with helium and passed over 200 mg of Au/$Ti(OH)_4^*$ at a flow rate of 67 ml min^{-1}. The partial pressures of reactants were varied from 0.25 to 3.5 kPa to obtain reaction orders at 263 K. CO_2 in effluent gas was analyzed by gas chromatography using a Carboxen 1000 column.

O_2 Temperature-Programmed Desorption

The catalysts were pretreated in the same manner as that mentioned above and exposed to 1.33 kPa of O_2 at room temperature for 30 min. Then the samples were evacuated for 20 min and the TPD measurement was carried out at a ramping rate of 10 K min^{-1} up to 673 K. The products evolved in the gas phase were analyzed using an on-line mass spectrometer.

FT-IR Spectra

FT-IR spectra were measured at room temperature on a JASCO FT/IR-230 spectrometer equipped with a MCT detector with a resolution of 4 cm^{-1}. Au/$Ti(OH)_4^*$ and TiO_2^* were pressed into self-supporting thin discs and placed in a quartz IR cell with CaF_2 windows, which was combined with a closed circulating system. The samples were pretreated in the quartz IR cell in a manner similar to that mentioned above, and exposed to CO or a mixture of $C^{16}O + {}^{32}O_2$ or $C^{16}O + {}^{36}O_2$ at room temperature. All the spectra were obtained by subtracting the spectra of gas phase CO and the samples before the gas exposure from the obtained spectra.

ESR Measurements

ESR spectra were recorded on a JEOL JES-RE2X ESR spectrometer at a frequency of 8.9 GHz at room temperature. DPPH (diphenylpicrylhydrazyl) was used as a reference ($g = 2.0036$) for determination of g values. The amount of paramagnetic species (spins/g) was determined by double integration of the area of resonance signals (after their overlap was resolved by computer simulation) and by calibration with a known amount of DPPH diluted (1000 : 1) with TiO_2^* (25–27). The catalyst samples were placed inside a quartz tube with a high-vacuum valve and calcined at 673 K under 13.3 kPa of O_2 and then evacuated at 673 K for 1 h before ESR measurements.

3. RESULTS

3.1. Oxygen Isotope Exchange

The oxygen isotope exchange of lattice oxygen atoms $^{16}O^*$ (*, lattice) with $^{36}O_2$ and the oxygen exchange in an equimolar mixture of $^{36}O_2 + {}^{32}O_2$ on Au/$Ti(OH)_4^*$ at 298 K are shown in Figs. 1a and 1b, respectively, where the fractions of three O_2 isotopomers, $^{16}O^{16}O$, $^{16}O^{18}O$, and $^{18}O^{18}O$, are plotted as a function of reaction time. Oxygen exchange reactions between gaseous $^{36}O_2$ and lattice oxygen $^{16}O^*$ and between gaseous $^{36}O_2$ and $^{32}O_2$ on Au/$Ti(OH)_4^*$ did not occur. The results indicate that the lattice oxygen atoms of Au/$Ti(OH)_4^*$ are not active in oxygen exchange and that oxygen molecules can not significantly dissociate to atomic oxygen on Au/$Ti(OH)_4^*$ at room temperature.

Figure 2 shows the oxygen isotope exchange of $C^{18}O$ with the lattice oxygen atom $^{16}O^*$ of Au/$Ti(OH)_4^*$ at 298 K. No isotope mixing in $C^{18}O$ occurred. Further, neither oxidation nor disproportionation of $C^{18}O$ was observed. The lattice oxygen atoms on the catalyst are inactive in both CO oxidation and oxygen exchange with CO.

Figure 3a shows that in the presence of gaseous $^{36}O_2$, $C^{16}O$ was rapidly oxidized and completely converted to carbon dioxide within 20 min. At the end of the reaction three kinds of CO_2 isotopomers, $C^{16}O^{16}O$, $C^{16}O^{18}O$, and

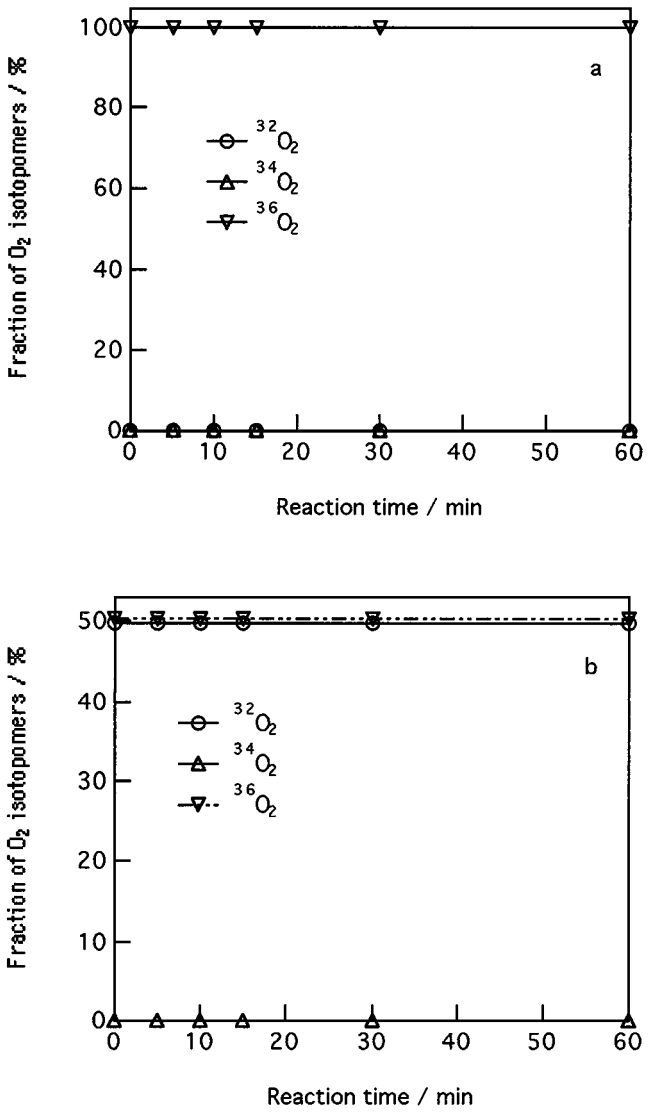

FIG. 1. Oxygen isotope exchange of lattice oxygen atoms of Au/Ti(OH)$_4^*$ with (a) $^{36}O_2$ and (b) an equimolar mixture of $^{32}O_2 + ^{36}O_2$. Cat., 0.1 g; Reaction temperature, 298 K.

$C^{18}O^{18}O$, with a molar ratio of about 1:2:1 were produced. No oxygen isotopomers ($^{16}O^{18}O$ and $^{18}O^{18}O$) were observed. As can be seen from Fig. 3b, no isotope mixing in O_2 and CO occurred during the reaction of CO and O_2, respectively (as in Figs. 1 and 2). It is indicated that the lattice oxygen atoms of Au/Ti(OH)$_4^*$ are not active in oxygen exchange and oxygen molecules do not dissociate to atomic oxygen on Au/Ti(OH)$_4^*$ during the CO oxidation. It is to be noted that $C^{16}O^{16}O$ and $C^{18}O^{18}O$ were formed during the reaction of $C^{16}O + ^{36}O_2$ and that $C^{18}O^{18}O$ was formed during the reaction of $C^{16}O + ^{32}O_2 + ^{36}O_2$ as shown in Figs. 3a and 3b.

The $C^{16}O$ oxidation with gaseous $^{36}O_2$ was also examined on TiO_2^*. $C^{16}O$ was not oxidized to carbon dioxide at room temperature, consistent with previous results (12). No oxygen mixing was observed either.

To clarify the origin of the three kinds of CO_2 isotopomers, $C^{16}O^{16}O$, $C^{16}O^{18}O$, and $C^{18}O^{18}O$, in Figs. 3a and 3b during the $C^{16}O$ oxidation in the presence of $^{36}O_2$, the oxygen exchange in CO_2 was examined (Figs. 4a and 4b). Figure 4a shows the oxygen exchange of $C^{18}O^{18}O$ with lattice oxygen $^{16}O^*$ on Au/Ti(OH)$_4^*$. $C^{18}O^{18}O$ rapidly exchanged with the lattice oxygen atom of the catalyst to form $C^{16}O^{18}O$ and the exchange reaction reached an equilibrium within 20 min. No $C^{16}O^{16}O$ was observed. In the presence of an equimolar mixture of $C^{16}O^{16}O$ and $C^{18}O^{18}O$, the exchange also took place very fast and reached an equilibrium within 10 min at a molar ratio of 1:2:1 for the three kinds of CO_2 isotopomers, $C^{16}O^{16}O$, $C^{16}O^{18}O$, and $C^{18}O^{18}O$, as shown in Fig. 4b. These results imply that the lattice oxygen atoms on Au/Ti(OH)$_4^*$ are very active in the oxygen exchange with CO_2.

Further, the oxygen exchange reactions between $C^{18}O$ and $C^{16}O^{16}O$ and between $C^{16}O^{16}O$ and $^{36}O_2$ on Au/Ti(OH)$_4^*$ were investigated at room temperature to determine the reactivity of adsorbed CO_2 in connection with the oxygen exchange mechanism. No oxygen exchange in these mixtures on Au/Ti(OH)$_4^*$ took place, as shown in Figs. 5 and 6, respectively.

3.2. *O_2 Temperature-Programmed Desorption*

Figure 7 (curve a) shows the O_2 TPD spectrum from the Au/Ti(OH)$_4^*$ sample exposed to oxygen (1.33 kPa) and evacuated at room temperature, in which O_2 was desorbed around 450 K. The amount of desorbed oxygen was 3.1 μmol g-cat^{-1}. When the catalyst was exposed to an equimolar mixture of $^{32}O_2$ and $^{36}O_2$, $^{32}O_2$ and $^{36}O_2$ were desorbed in a similar manner, where no desorption of $^{16}O^{18}O$ was detected using a quadruple mass spectrometer, indicating no dissociative adsorption of O_2.

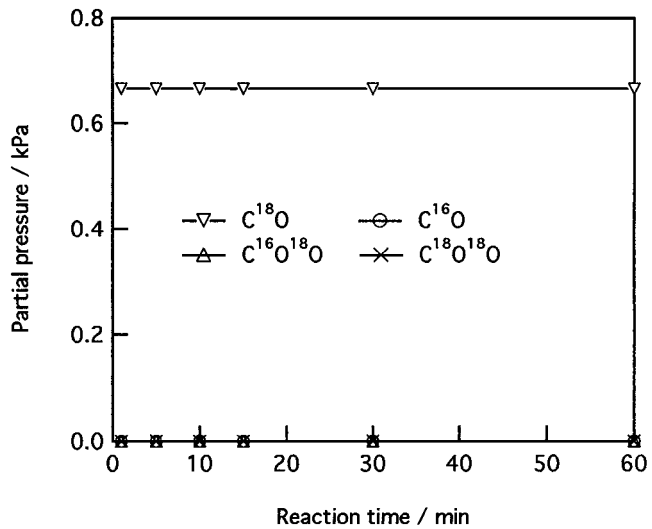

FIG. 2. $C^{18}O$ oxidation and oxygen isotope exchange on Au/Ti(OH)$_4^*$ at 298 K in the absence of gaseous oxygen. Cat., 0.1 g.

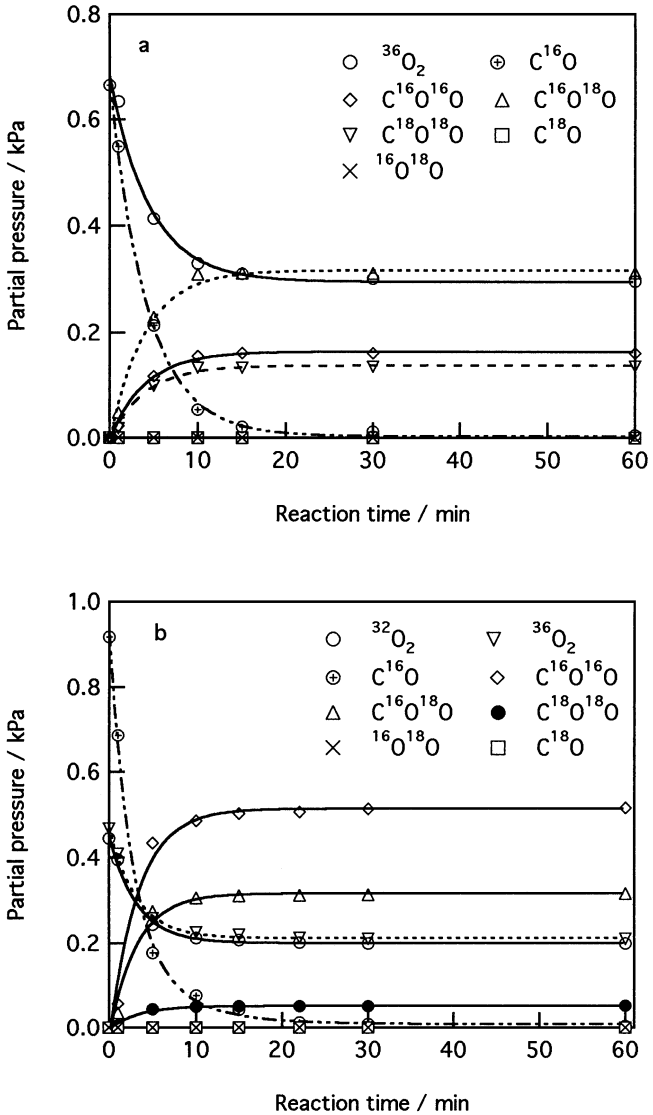

FIG. 3. Oxygen isotope distributions during (a) $C^{16}O$ (0.67 kPa) oxidation with $^{36}O_2$ (0.67 kPa) and (b) $C^{16}O$ (0.92 kPa) oxidation with a mixture of $^{32}O_2 + {}^{36}O_2$ (0.46 kPa for each) on Au/Ti(OH)$_4^*$ at 298 K (0.92 kPa for CO). Cat., 0.1 g.

The reaction of adsorbed oxygen with CO was performed by addition of CO pulse to the Au/Ti(OH)$_4^*$ sample exposed to O_2 and evacuated at room temperature for 30 min. As shown in Fig. 7 (curves b–d), increasing the amount of CO decreased the O_2-TPD peak. When 0.67 kPa of CO was admitted to the system, the oxygen desorption peak disappeared. The results suggest that all the adsorbed oxygen species on Au/Ti(OH)$_4^*$ are active in CO oxidation at room temperature.

3.3. *Annealing Effects on Au/Ti(OH)$_4^*$*

The O_2 TPD was performed on an annealed Au/Ti(OH)$_4^*$ sample (Fig. 8, curve c). Oxygen seems to hardly adsorb on the annealed Au/Ti(OH)$_4^*$ surface, where the amount of desorbed oxygen was as small as 0.2 μmol g-cat^{-1}.

Figure 9 shows the activity of the annealed Au/Ti(OH)$_4^*$ catalyst in CO oxidation. The initial rate of CO oxidation decreased about 10 times compared with that on nonannealed Au/Ti(OH)$_4^*$. The results shown in Figs. 8 and 9 reveal that the properties of Au/Ti(OH)$_4^*$ strongly depend on the pretreatment conditions.

3.4. *Electron Spin Resonance for Au/Ti(OH)$_4^*$ and TiO$_2^*$ after O_2 Adsorption*

To obtain information on the state of the adsorbed oxygen species, ESR spectra for Au/Ti(OH)$_4^*$ and TiO$_2^*$ after O_2 adsorption were recorded at room temperature. As shown in Fig. 10, Au/Ti(OH)$_4^*$ evacuated at 673 K gave a symmetric signal at $g = 2.002$. Upon oxygen adsorption on

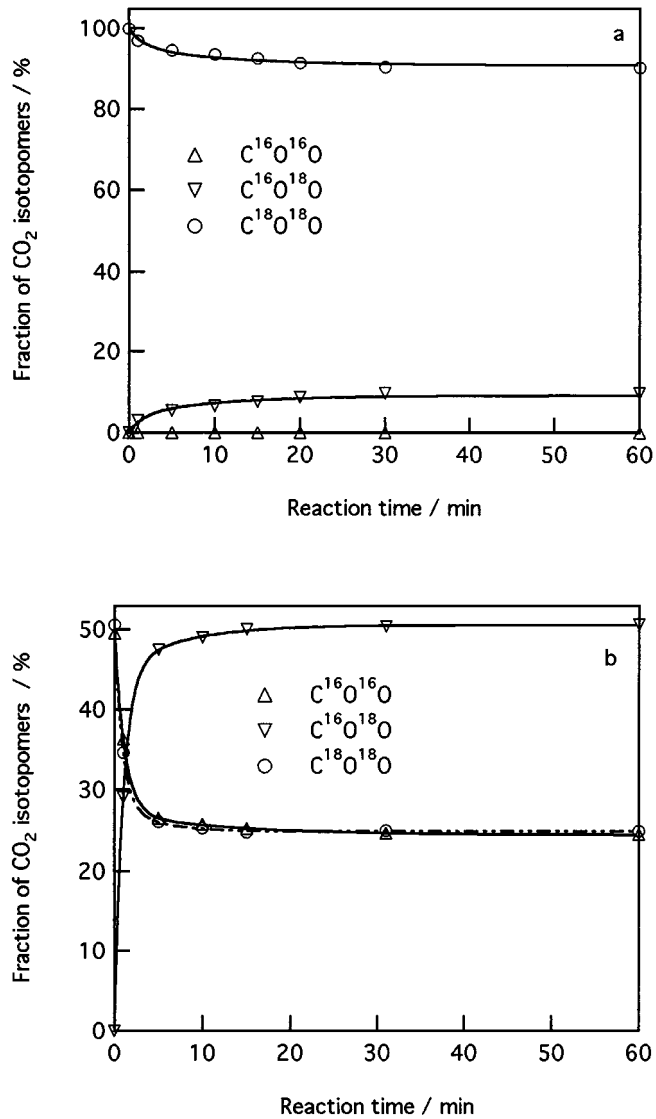

FIG. 4. Oxygen isotope exchange in carbon dioxide on Au/Ti(OH)$_4^*$ at 298 K: (a) $C^{18}O^{18}O$ (0.67 kPa) and (b) a mixture of $C^{16}O^{16}O + C^{18}O^{18}O$ (0.40 kPa for each). Cat., 0.1 g.

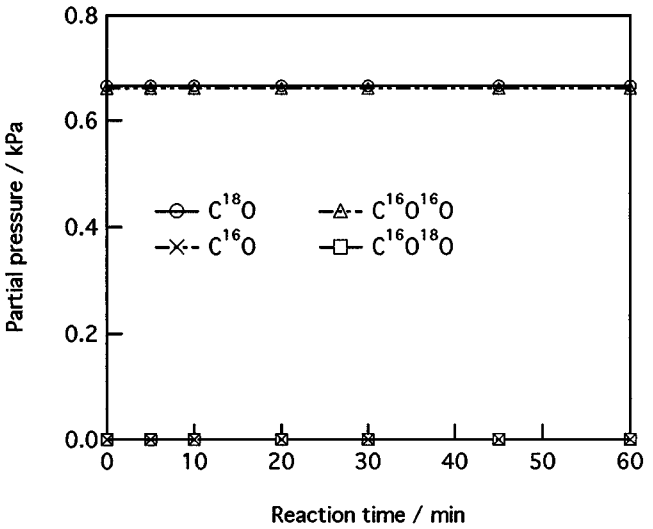

FIG. 5. Oxygen isotope exchange under a mixture of $C^{16}O^{16}O + C^{18}O$ (0.67 kPa for each) on Au/Ti(OH)$_4^*$ at 298 K. Cat., 0.1 g.

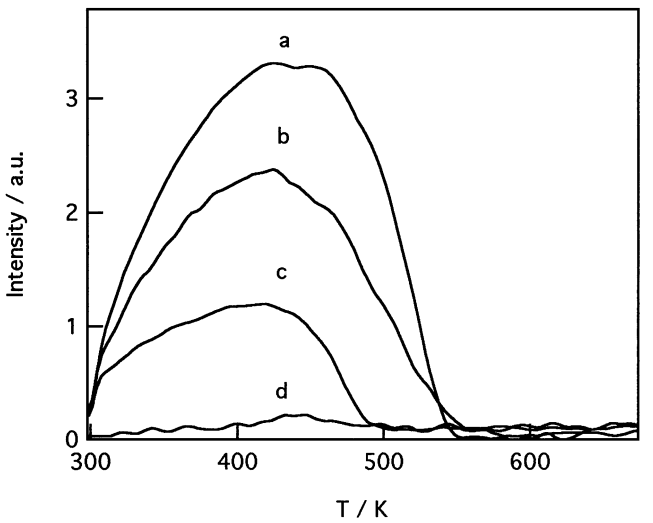

FIG. 7. O_2-TPD on Au/Ti(OH)$_4^*$: (a) after exposure to 1.33 kPa of $^{32}O_2$ and evacuation at 298 K; (b), (c), and (d) after addition of 0.03, 0.06, and 0.67 kPa of CO pulse to (a) at 298 K, respectively; Cat. 0.1 g.

Au/Ti(OH)$_4^*$ followed by evacuation at room temperature, new peaks were observed, while the intensity of the peak at $g = 2.002$ decreased. The new peaks were characterized as $g_1 = 2.020$, $g_2 = 2.010$, and $g_3 = 2.005$, which are characteristic of superoxide O_2^- radicals with an angular arrangement (28–32). The amount of the paramagnetic O_2^- species was estimated to be 1.8 μmol g^{-1}. Subsequent exposure of the O_2-adsorbed catalyst to 2.2 kPa of CO at room temperature resulted in a progressive diminution of the signal intensity and a simultaneous increase in the initial signal at $g = 2.002$ (Fig. 10, curves c–e). All the adsorbed O_2^- species reacted with CO.

On an annealed Au/Ti(OH)$_4^*$ sample O_2 adsorption produced a very small amount of O_2^- species (0.04 μmol g^{-1}) as shown in Fig. 10 (curve f).

Figure 11 shows ESR spectra for TiO_2^* evacuated at 673 K and exposed to CO at room temperature. The evacuated TiO_2^* gave two signals at $g = 2.003$ and 1.980, due to F centers and Ti^{3+}, respectively (28, 29, 33–35). After O_2 adsorption on the TiO_2^* these two signals disappeared, while an O_2^- signal appeared with three g values of 2.027, 2.010, and 2.004 (Fig. 11, curve b) also corresponding to the angular arrangement. The amount of O_2^- radicals was 0.5 μmol g^{-1}. Exposure to CO did not influence the O_2^- spectrum

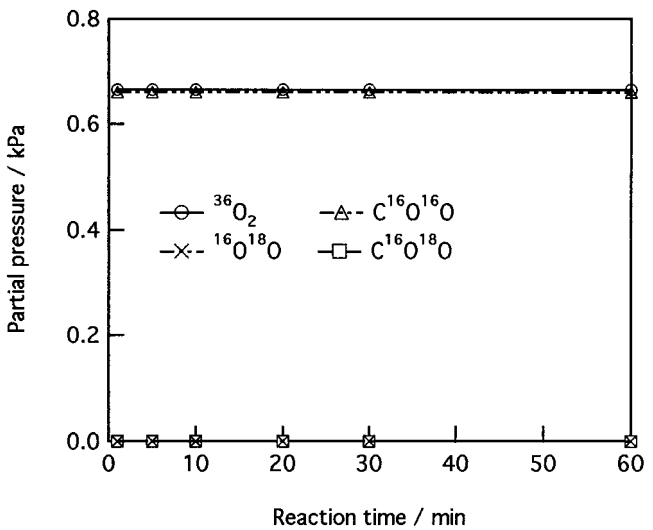

FIG. 6. Oxygen isotope exchange under a mixture of $C^{16}O^{16}O + {}^{36}O_2$ (0.67 kPa for each) on Au/Ti(OH)$_4^*$ at 298 K. Cat., 0.1 g.

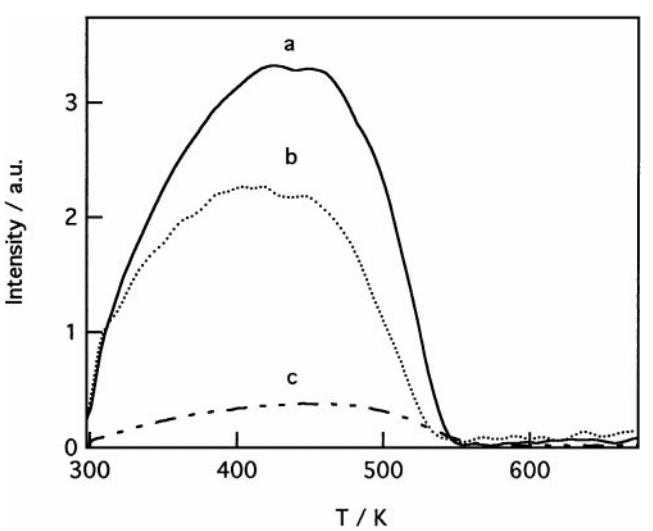

FIG. 8. O_2-TPD on Au/Ti(OH)$_4^*$ (a), TiO_2^* (b), and annealed Au/Ti(OH)$_4^*$ (c). Cat., 0.1 g.

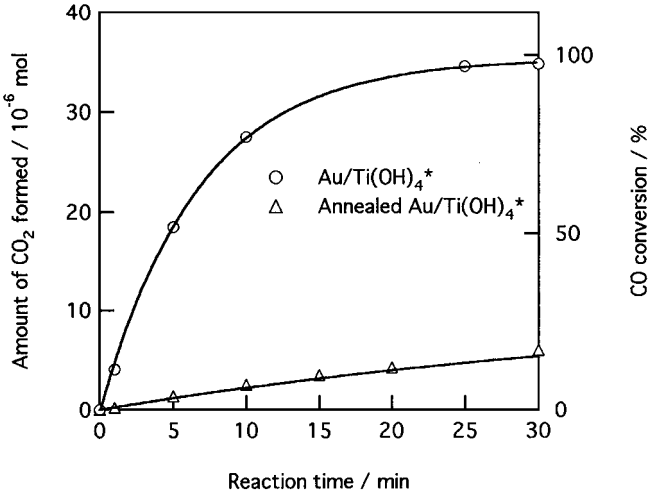

FIG. 9. Annealing effect of Au/Ti(OH)$_4^*$ on CO oxidation at 298 K. Cat., 0.04 g.

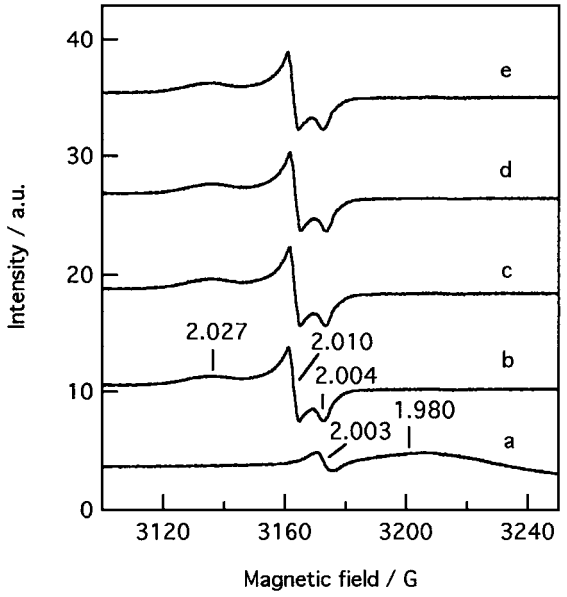

FIG. 11. ESR spectra for TiO_2^* at room temperature: (a) after evacuation at 673 K; (b) after exposure to 1.33 kPa of O_2 followed by evacuation; (c), (d), and (e) after subsequent exposure to 2.13 kPa of CO at room temperature for 10, 28, and 60 min, respectively.

as shown in Fig. 11, indicating no reaction between the adsorbed O_2 and CO on TiO_2^*.

3.5. FT-IR Spectra for Adsorbed CO

Figure 12 shows FT-IR spectra of CO adsorbed on Au/Ti(OH)$_4^*$. The spectra (a–d) were recorded at 10 min after CO introduction at room temperature. Three bands were observed at 2188, 2136, and 2119 cm^{-1} in the range 2400–1800 cm^{-1}. With decreasing CO pressure, the three bands decreased in intensity. After evacuation of CO at room temperature for 2 min, only a 2136 cm^{-1} adsorption peak was detected (spectrum e), and further evacuation for 10 min resulted in complete disappearance of the three

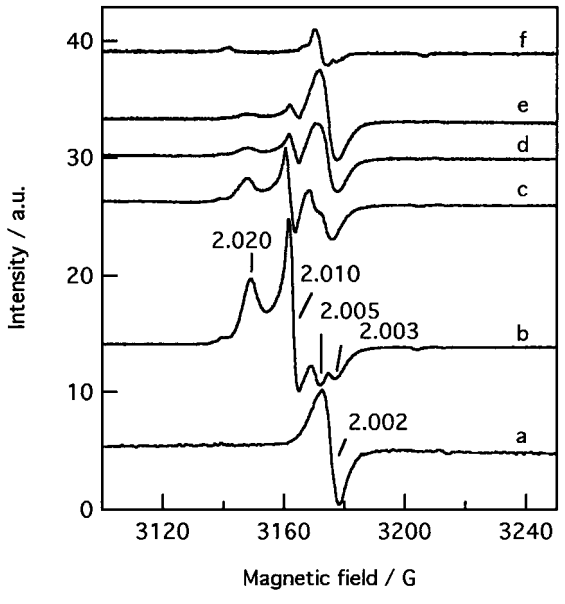

FIG. 10. ESR spectra for Au/Ti(OH)$_4^*$ at room temperature: (a) after evacuation at 673 K; (b) after exposure to 1.33 kPa of O_2 followed by evacuation; (c), (d) and (e) after subsequent exposure to 2.13 kPa of CO at room temperature for 10, 28, and 60 min, respectively. (f) ESR spectrum for oxygen (1.33 kPa)-adsorbed, annealed Au/Ti(OH)$_4^*$.

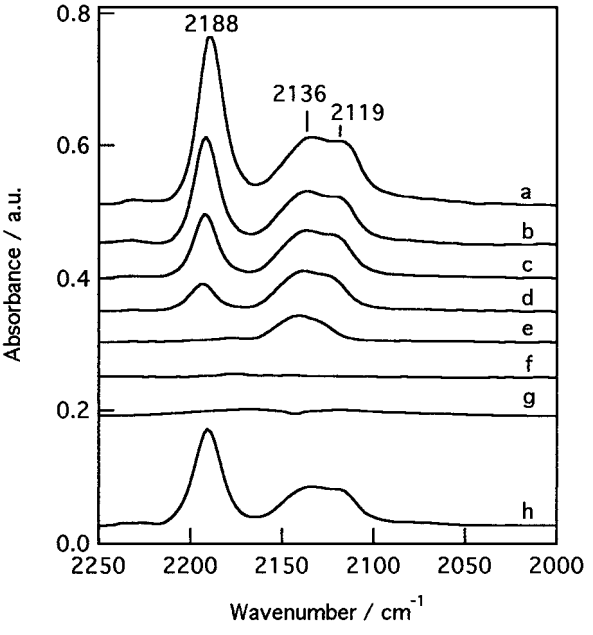

FIG. 12. FT-IR spectra of CO adsorbed on Au/Ti(OH)$_4^*$ at 298 K at (a) 6.65 kPa, (b) 2.66 kPa, (c) 0.67 kPa, and (d) 0.266 kPa; (e) after 2 min of evacuation; and (f) after 10 min of evacuation. FT-IR spectra of (g) CO adsorbed on TiO_2^* at 2.66 kPa and (h) CO adsorbed on annealed Au/Ti(OH)$_4^*$ at 2.66 kPa.

bands (spectrum f), showing reversible CO adsorption on Au/Ti(OH)$_4^*$. After 2 min of evacuation, 0.67 kPa of O_2 was admitted to the system, and the band at 2136 cm^{-1} rapidly disappeared (not shown in Fig. 12).

Figure 13 shows the dependence of the integrated intensities of the CO absorption bands at 2188 and 2136 + 2119 cm^{-1} on the CO pressure. The intensity of the band at 2188 cm^{-1} (assigned to CO on Ti^{4+} as discussed later) increased with an increase in CO pressure. The intensity of the bands at 2136 and 2119 cm^{-1} (assigned to CO on Au as discussed later) saturated nearly at the CO pressure of 1.0 kPa.

On the TiO_2^* support, no band for adsorbed CO was observed (curve g in Fig. 12). Thus Au particles seem to affect the state of the Ti^{4+} sites for CO adsorption on the support. Annealing of Au/Ti(OH)$_4^*$ under 13.3 kPa of O_2 did not affect the CO adsorption capability of Au/Ti(OH)$_4^*$ as shown in Fig. 12, spectrum h, which is almost identical to spectrum b of Fig. 12 for Au/Ti(OH)$_4^*$.

FT-IR spectra of adsorbed CO in the presence of $^{32}O_2$ or $^{36}O_2$ are shown in Fig. 14. In the range 1800–1200 cm^{-1}, two weak peaks at 1570 and 1320 cm^{-1} appeared after admission of 2.66 kPa of CO alone (Fig. 14, spectrum a). The two peaks are assigned to bidentate carbonate species (9, 36). Only a limited number of lattice oxygen atoms reacted with CO to form surface carbonates that remained at the surface without decomposition to gaseous CO_2, as those lattice oxygen atoms were not replenished by bulk oxygen. The presence of $^{32}O_2$ reduced the intensity of three CO bands at 2188, 2136, and 2119 cm^{-1}, whereas in contrast to the literature (22, 37) no shifts in these bands were observed. After admission of CO + $^{32}O_2$ for 5 min (Fig. 14, spectrum b) in a closed circulating system, the remaining CO pressure became about 1.2 kPa. The integrated intensities of the three CO peaks were plotted also in Fig. 13. The intensity of the CO peak at 2188 cm^{-1} was in agreement with the adsorption isotherm of CO on Ti^{4+}, whereas the peak intensity of CO adsorbed on Au particles at 2136 + 2119 cm^{-1} was significantly smaller than the corresponding CO adsorption isotherm. Along with the reduction of CO bands, bands of adsorbed CO_2 around 2350 cm^{-1} appeared and increased with reaction time, indicating the formation of CO_2 by reaction of CO adsorbed on Au particles with O_2. The bands around 2350 cm^{-1} were due to the asymmetric stretching of CO_2 molecules (9, 22). Production of the carbonate species (1200–1600 cm^{-1}) was much greater compared to the production in the absence of O_2 as shown in Fig. 14. After gaseous O_2 was completely consumed, further introduction of CO did not affect the bands of carbonate species (spectra c and d in Fig. 14). Replacement of $^{32}O_2$ by $^{36}O_2$ caused shifts of the carbonate peaks to lower frequencies by about 15 cm^{-1} (Fig. 14, spectrum e). This is compatible with the result that the oxygen exchange between $C^{16}O^{16}O$ and $C^{18}O^{18}O$, probably through carbonates, was very rapid as shown in Fig. 4.

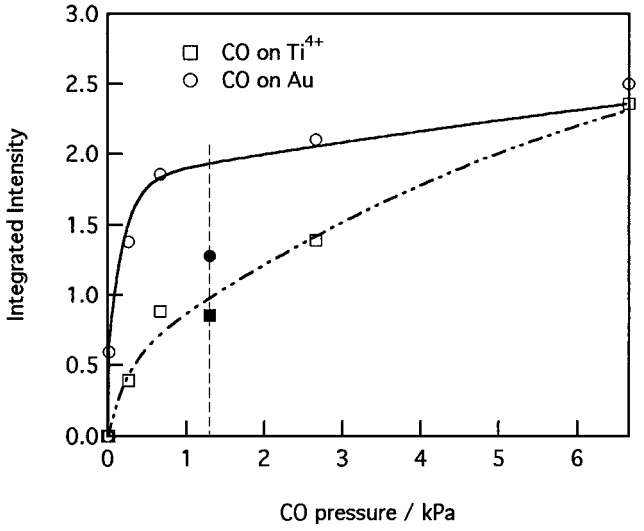

FIG. 13. Integrated intensities of the ν_{CO} bands at 298 K as a function of CO pressure; ● and ■ repersent the integrated intensities of CO adsorption on Au and Ti^{4+}, respectively, after admission of CO + O_2 on Au/Ti(OH)$_4^*$ as shown in Fig. 14 (curve b).

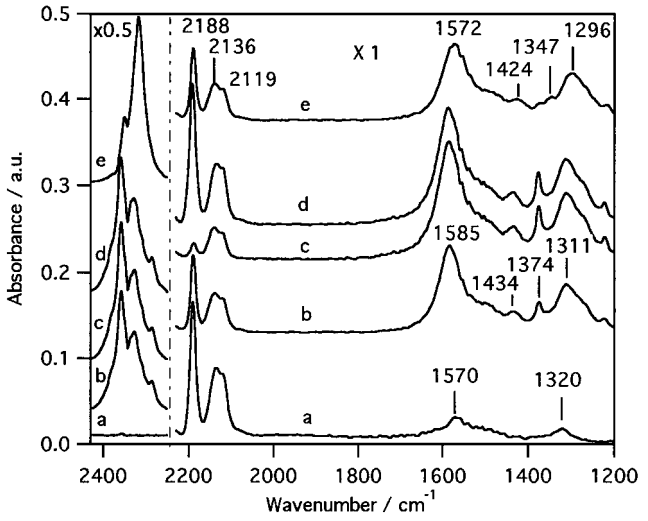

FIG. 14. FT-IR spectra of CO adsorbed on Au/Ti(OH)$_4^*$ at 298 K after admission of 2.66 kPa of CO (a), admission of 2.66 kPa of CO + 1.20 kPa of $^{32}O_2$ for 5 min (b) and 20 min (c), and subsequent admissions of 2.66 kPa of CO (d) and 2.66 kPa of CO + 1.60 kPa of $^{36}O_2$ (e).

4. DISCUSSION

It has been demonstrated that the Au/Ti(OH)$_4^*$ catalysts prepared from Au(PPh$_3$)(NO$_3$) and as-precipitated wet Ti hydroxide were much more active for low-temperature CO oxidation compared with TiO_2-supported Au catalysts prepared by traditional impregnation methods (11–13). The

developed Au/Ti$(OH)_4^*$ catalyst was active in CO oxidation and exhibited 50% conversion (4.47×10^{-3} mol/h/g-cat) at room temperature in a steady-state flow reactor system (20,000 ml/h/g; CO, 1.0%; balanced with air at atmospheric pressure).

As possible reaction mechanisms for the catalytic oxidation of CO with O_2 on Au/Ti$(OH)_4^*$, we assume the following six mechanisms at the catalyst surface (a, adsorbed species); (1) reaction of CO (a) with active surface lattice oxygen O^* ($CO\,(a) + O^* \rightarrow CO^*O$ and $1/2\ O_2 \rightarrow O^*$), (2) reaction of CO (a) with active oxygen atoms O^* produced by dissociation of gaseous O_2 at defect sites of the support surface ($1/2\,O_2 \rightarrow O^*$, and $O^* + CO \rightarrow CO_2$), (3) reaction of CO (a) with adsorbed molecular oxygen O_2^* ($2\,CO\,(a) + O_2^* \rightarrow 2\,CO_2$), (4) reaction of CO (a) with O_2^* to form carbonate CO_3, followed by reaction of produced CO_3 with CO (a) ($CO\,(a) + O_2{}^* \rightarrow CO_3\,(a)$, $CO_3\,(a) + CO\,(a) \rightarrow 2\,CO_2$), (5) reaction of CO (a) with ozonate species O_3^* that may be produced by O_2 and O^* ($O_2 + O^* \rightarrow O_3^*$, $O_3^* + CO\,(a) \rightarrow CO_2 + O_2$), and (6) disporptionation of CO (a) to produce $CO_2 + C$ (a), followed by oxidation of C (a) with O_2 ($2\,CO\,(a) \rightarrow CO_2 + C\,(a)$, $C\,(a) + O_2 \rightarrow CO_2$). We discuss here a most probable mechanism for the low-temperature CO oxidation on the Au/Ti$(OH)_4^*$ catalyst on the basis of oxygen isotope exchange, O_2 TPD, ESR for adsorbed oxygen species, and FT-IR for adsorbed CO.

Irrespective of a high catalytic oxidation activity of the Au/Ti$(OH)_4^*$ catalyst in CO oxidation with O_2 at room temperature, the surface lattice oxygen atoms O^* of the Au/Ti$(OH)_4^*$ catalyst were unreactive to both CO and O_2 as shown in Fig. 2 (Eq. [1]) and Fig. 1a (Eq. [2]).

$$C^{18}O + {}^{16}O^* \rightarrow C^{16}O^{18}O \text{ (no reaction).} \quad [1]$$

$$^{36}O_2 + {}^{16}O^* \rightarrow {}^{16}O^{18}O + {}^{18}O^* \text{ (no oxygen exchange).} \quad [2]$$

These results exclude Mechanism (1). One can say that adsorbed CO_2 produced by CO and O^* might be converted to CO again ($CO + O^* \rightarrow COO^* \rightarrow CO^* + O$) even when the adsorbed CO_2 is not desorbed to the gas phase. But this may be denied by the result shown in Fig. 2, which shows no oxygen mixing between $C^{18}O$ and ${}^{16}O^*$ to produce $C^{16}O$ (Eq. [3]).

$$C^{18}O + {}^{16}O^* \rightarrow C^{16}O + {}^{18}O^* \text{ (no oxygen exchange).} \quad [3]$$

No $C^{18}O^{18}O$ was formed in Reaction [1], which implies that disproportionation of $C^{18}O$ (Eq. [4]) does not occur on the catalyst, excluding Mechanism (6).

$$2\,C^{18}O \rightarrow C + C^{18}O^{18}O \text{ (no reaction).} \quad [4]$$

As can be seen from Fig. 1a, it is likely that O_2 does not dissociate to oxygen atoms because if O_2 dissociated to oxygen atoms oxygen isotope mixing would take place on the surface. The results do not show this to be the case. Alternatively, a limited number of active oxygen atoms may be isolated on the surface and hence ${}^{16}O^{18}O$ may not be observed. However, this is unlikely as oxygen exchange between $^{36}O_2$ and $^{32}O_2$,

$$^{32}O_2 + {}^{36}O_2 \rightarrow {}^{16}O^{18}O \text{ on } {}^{16}O^* \text{ (no oxygen exchange),} \quad [5]$$

did not occur (Fig. 1b), because even if the active oxygen atoms were very few, ${}^{16}O^{18}O$ should be detected after the prolonged catalytic $^{32}O_2 + {}^{36}O_2$ exchange reaction. Further, that there is no oxygen scrambling between $^{32}O_2$ and $^{36}O_2$ on Au/Ti$(OH)_4^*$ (Eq. [5]) and no finding of ${}^{16}O^{18}O$ in the system $^{36}O_2 + {}^{16}O^*$ (Eq. [2]) also indicates no formation of ozonate species O_3^* as a reaction intermediate, which may exclude Mechanism (5), because if O_3^* species had been produced by gaseous oxygen molecules and surface oxygen atoms, oxygen isotope scrambling would have been observed. Mechanism (2) is also unlikely because there is no oxygen isotope exchange in Eq. [5].

In the reaction of $C^{16}O$ and $^{36}O_2$ on Au/Ti$(OH)_4^*$,

$$C^{16}O + {}^{36}O_2 \rightarrow C^{16}O^{18}O, C^{16}O^{16}O, \text{ and } C^{18}O^{18}O. \quad [6]$$

neither oxygen exchange in $C^{16}O$ nor that in $^{36}O_2$ took place, as shown in Fig. 3a,

$$C^{16}O + {}^{36}O_2 \rightarrow C^{18}O + {}^{16}O^{18}O \text{ (no oxygen exchange).} \quad [7]$$

Figure 3a reveals that the reaction from $C^{18}O^{18}O$ or $C^{16}O^{18}O$ to $C^{18}O$ (backward reaction in Mechanism (4)) never proceeded on the catalyst. We expected the formation of $C^{16}O^{18}O$ alone as the product of Reaction [6], but lots of $C^{16}O^{16}O$ and $C^{18}O^{18}O$ were produced. As CO and O_2 molecules themselves did not contribute to oxygen isotope mixing processes on Au/Ti$(OH)_4^*$ as discussed above, the oxygen exchange in carbon dioxide may be due to an isotope scrambling by the secondary reaction of $C^{16}O^{18}O$ produced first from $C^{16}O$ and $^{36}O_2$ (Eq. [8]). The disproportionation of $C^{16}O^{18}O$,

$$2\,C^{16}O^{18}O \rightarrow C^{16}O^{16}O \text{ and } C^{18}O^{18}O, \quad [8]$$

may proceed via carbonates that are observed at the catalyst surface under the catalytic reaction conditions as shown in Fig. 14. The carbon dioxide isotopomers $C^{16}O^{18}O$, $C^{16}O^{16}O$, and $C^{18}O^{18}O$ were also produced in the reaction $C^{16}O + {}^{32}O_2 + {}^{36}O_2$,

$$C^{16}O + {}^{32}O_2 + {}^{36}O_2 \rightarrow C^{16}O^{18}O, C^{16}O^{16}O \text{ and } C^{18}O^{18}O, \quad [9]$$

as shown in Fig. 3b. While $^{32}O_2$ and $^{36}O_2$ were consumed in a ratio of approximately 1 : 1 during the CO oxidation, the amount of produced $C^{16}O_2$ was much larger than that of $C^{16}O^{18}O$ and the amount of produced $C^{18}O^{18}O$ was much

lower than that of the others (Fig. 3b). This can also be explained by the secondary disproportionation reaction of the produced $C^{16}O^{18}O$ (Eq. [8]).

To examine the behavior of produced CO_2 on Au/Ti(OH)$_4^*$, the oxygen exchange reactions between carbon dioxide and lattice oxygen atoms and between two carbon dioxide isotopomers were investigated (Fig. 4). $C^{18}O^{18}O$ rapidly reacted with lattice $^{16}O^*$ atoms to form $C^{16}O^{18}O$ by a single oxygen exchange, as shown in Fig. 4a (Eq. [10]), and the oxygen atoms of $C^{16}O^{16}O$ and $C^{18}O^{18}O$ rapidly exchanged with each other to form $C^{16}O^{18}O$, as shown in Fig. 4b (Eq. [11]). The rates of the oxygen exchange reactions (Eq. [10] and Eq. [11]) were so fast that we could not estimate the initial rates under the present conditions in a closed circulating system. Thus, the population of oxygen carbon dioxide isotopomers observed in Fig. 3 is assigned to the rapid disproportionation of the produced carbon dioxide.

$$C^{18}O^{18}O + {}^{16}O^* \rightarrow C^{16}O^{18}O + {}^{18}O^*. \quad [10]$$

$$C^{16}O^{16}O + C^{18}O^{18}O \rightarrow 2\,C^{16}O^{18}O. \quad [11]$$

To examine the possibility that Mechanism (4) involves the reaction of carbonate with CO, the oxygen isotope exchange between $C^{18}O$ and $C^{16}O^{16}O$,

$$C^{18}O + C^{16}O_2 \rightarrow C^{16}O + C^{16}O^{18}O \text{ (no reaction)}, \quad [12]$$

on Au/Ti(OH)$_4^*$ was monitored (Fig. 5) and no isotope scrambling in either $C^{18}O$ or $C^{16}O^{16}O$ was observed. Because the oxygen atom of $C^{16}O^{16}O$ is assumed to rapidly exchange with the lattice oxygen atom $^{16}O^*$ on Au/Ti(OH)$_4^*$ via carbonate $C^{16}O^{16}O^{16}O$ as discussed above, if the carbonate species behaved as a reaction intermediate for the catalytic CO oxidation, $C^{16}O^{18}O$ would be produced by the reaction of $C^{16}O^{16}O^{16}O$ and $C^{18}O$. The results shown in Fig. 5 imply that the catalytic CO oxidation with O_2 to form CO_2 does not take place by the two successive steps $CO + O_2 \rightarrow CO_3$ and $CO_3 + CO \rightarrow 2\,CO_2$, which may exclude Mechanism [4].

Under the catalytic reaction conditions, carbonate peaks at 1585 and 1311 cm^{-1} (assigned to bidentate carbonates), 1374 cm^{-1} (unidentate carbonate), and 1434 cm^{-1} (uncoordinated carbonate) (9, 21, 22, 36) in Fig. 14 (curve c) did not change by CO introduction (Fig. 14, curve d), indicating no reaction of the surface carbonates with CO to form gaseous CO_2, which also excludes Mechanism [4]. Carbonate species do not appear to be an active intermediate for the low-temperature CO oxidation, which is quite different from the previous proposal of Haruta *et al.* on Au/TiO_2 and Au/ZnO (4, 5, 22, 37).

To further examine the reactivity of adsorbed CO_2 or CO_3 on Au/Ti(OH)$_4^*$, the oxygen isotope exchange experiments,

$$^{36}O_2 + C^{16}O^{16}O \rightarrow {}^{16}O^{18}O + C^{16}O^{18}O$$

(no oxygen exchange), [13]

were performed at room temperature. If $^{36}O_2$ dissociates to ^{18}O on the catalyst surface, the produced ^{18}O atoms should react with $C^{16}O^{16}O$ to form the carbonate $C^{16}O^{16}O^{18}O$ and hence oxygen scrambling in CO_2 will be observed as shown in Fig. 4a. However, Fig. 6 shows no oxygen exchange between $^{36}O_2$ and $C^{16}O^{16}O$, where neither $^{16}O^{18}O$ nor $C^{16}O^{18}O$ were observed, suggesting no dissociation of O_2 on the Au/Ti(OH)$_4^*$ catalyst.

All the data discussed above reveal that O_2 does not dissociate to oxygen atoms on the catalyst surface at room temperature. ESR spectra in Fig. 10 provide additional evidence for the presence of molecular oxygen species on the Au/Ti(OH)$_4^*$ catalyst exposed to O_2 at room temperature. The signal at $g = 2.002$ observed with the catalyst after evacuation at 673 K may be assigned to oxygen vacancies (F centers) of the Ti oxide surfaces (29, 33, 34). The similar signal on a TiO_2 has been attributed to O^- (38). However, this assignment does not fit the present case because O^- is known to be active in oxygen exchange and also in CO oxidation (28, 31, 32), whereas any oxygen isotope exchange did not occur on the surface with the signal of $g = 2.002$ (Eq. [2]). The signal intensity decreased by O_2 adsorption, accompanied by the appearance of signals with $g_1 = 2.020$, $g_2 = 2.010$, and $g_3 = 2.005$ which are assigned to an angular arrangement of superoxide O_2^- adsorbed on a Ti cation, $Ti^{4+}\diagup\!\!\diagdown^{O}_{O^-}$ as shown in Fig. 10 (spectrum b) (28–32). The O_2^- species was consumed by reaction with CO, accompanied by an increase in the signal of $g = 2.002$ in Fig. 10 (spectra c–e). Thus, it is most likely that O_2 was adsorbed on the oxygen vacancies ($g = 2.002$) to form superoxide O_2^- radicals with the angular conformation. The adsorbed oxygen desorbed below 550 K as shown in the TPD of Fig. 7. Oxygen species on TiO_2, ZnO, and Fe_2O_3 that desorb below 573 K have been assigned to superoxide O_2^- (39). All the adsorbed O_2^- species reacted with CO as shown in Fig. 7. The O_2^- species that desorb at the higher temperature TPD spectra seem to have higher reactivity to CO, possibly due to the stronger interaction with Ti^{4+} ions leading to more activation of the O_2^- species. From the TPD the amount of adsorbed oxygen was estimated to be 1.9×10^{18} oxygen molecules g-cat^{-1} on Au/Ti(OH)$_4^*$. If we assume that the number of Ti^{4+} ions exposed to the surface is an order of 10^{20} Ti g-cat^{-1}, the amount of adsorbed oxygen is as few as 1% of the exposed Ti^{4+} ions. The amount of O_2^- estimated by the ESR signal is about 60% of that estimated by the TPD spectrum. The difference may be referred to a large error bar in the estimation by ESR. A part of adsorbed oxygen molecules may be undetectable by ESR and desorb at the lower temperature in TPD.

The annealed Au/Ti(OH)$_4^*$ catalyst was much less active than the Au/Ti(OH)$_4^*$ catalyst in CO oxidation at room temperature as shown in Fig. 9. On the annealed catalyst O_2 adsorption was much less than that on the Au/Ti(OH)$_4^*$ catalyst as shown in Fig. 8, which may be the major reason for the low oxidation activity of the annealed sample. The produced O_2^- species on the annealed catalyst showed $g_1 = 2.025$, $g_2 = 2.005$, and $g_3 = 1.980$ (tentative), which is different from the g values observed with the Au/Ti(OH)$_4^*$ catalyst, corresponding to a perpendicular arrangement Ti^{4+}--$\begin{matrix} O^- \\ | \\ O \end{matrix}$ (29).

Oxygen also adsorbed on the TiO_2^* sample without Au as shown in Fig. 8. The desorption peak pattern was similar to that for the Au/Ti(OH)$_4^*$ catalyst. The presence of Au has a positive effect on O_2 adsorption as shown in Fig. 8. The amount of O_2^- detected by ESR was about 3.5 times more on the Au/Ti(OH)$_4^*$ catalyst than on the TiO_2^* sample (Figs. 10 and 11). The addition of Au promotes the formation of superoxide O_2^- bound to Ti^{4+}. The g_1 value for O_2^- on TiO_2^* shifted to the lower field compared with that on Au/Ti(OH)$_4^*$. The low-field g_1 value among the g tensor parameters for O_2^- species is known to be most sensitive to the electric charge of the adsorption center and the environment of the electric field (31, 32). We think that during the preparation of the Au/Ti(OH)$_4^*$ catalyst from Au–phosphine complex precursor and as-precipitated Ti hydroxide precursor by thermal decomposition in air, the presence of Au species facilitates the formation of oxygen defects on the Ti oxide surface at the boundary of Au particles, where oxygen molecules adsorb as O_2^- bound to coordinatively unsaturated Ti^{4+} ions. Similar phenomena were observed on CeO_2/Al_2O_3 (33), $Pt/CeO_2/Al_2O_3$ (34, 40), V_2O_5/ZrO_2 (31), and Ru/ZnO (41). Neither O_2^- reaction with CO (Fig. 11) nor CO adsorption on TiO_2^* (Fig. 12, curve g) occurred, which is in agreement with the observation that no catalytic CO oxidation proceeded on TiO_2^* at room temperature.

On supported Au catalysts several CO adsorption sites have been characterized by FT-IR: CO adsorbed on Au particle surfaces (9, 21–24, 42) with $\nu_{CO} = 2105$–$2134\ cm^{-1}$, CO adsorbed on positively charged Au sites (19, 22) with $\nu_{CO} = 2154$–$2159\ cm^{-1}$, CO adsorbed on the perimeters of Au particles (22) with $\nu_{CO} = 2090$–$2110\ cm^{-1}$, and CO coadsorbed with oxygen on neighboring Au sites (19, 22, 23) with $\nu_{CO} = 2133$–$2138\ cm^{-1}$. Additionally, the bands due to interaction of CO with M^{n+} sites and/or OH groups of a support have also been observed (22–24). The band at $2188\ cm^{-1}$ in Fig. 12 can be assigned to linear CO on Ti^{4+} (9, 21, 22, 43), and the band at $2119\ cm^{-1}$ can be assigned to linear CO on Au metallic particles (4, 5, 9, 14, 19, 21, 22, 44). As for the band at $2136\ cm^{-1}$, it is tentatively assigned to CO on Au metallic particles strongly interacting with the support surface though it was blue-shifted by $17\ cm^{-1}$ from the $2119\ cm^{-1}$ band (44). Fraissard *et al.* (45) observed a peak at about $2140\ cm^{-1}$ for strongly adsorbed CO on $[Au]_n^{\delta+}$ particles in HY zeolite. This peak remained after evacuation for 30 min at room temperature. The feature is entirely different from the present one for the $2136\ cm^{-1}$ peak on Au/Ti(OH)$_4^*$. The $2136\ cm^{-1}$ peak can not be assigned to CO adsorbed on oxidized gold sites because there is no information on the presence of oxidized Au sites on the Au/Ti(OH)$_4^*$ catalyst as discussed in the previous paper (46). CO reversibly adsorbs on Ti^{4+} ions and Au particles on the Au/Ti(OH)$_4^*$ catalyst. Upon O_2 adsorption (Fig. 14, curve b), the frequencies did not shift. In a mixture of $C^{16}O$ and $^{36}O_2$, no band for $C^{18}O$ was observed (Fig. 14, curve e) coinciding with no oxygen isotope exchange in Fig. 3a. These results are entirely different from the results on the Au/TiO_2 and Au/ZnO catalysts, where blue shift of ν_{CO} peaks was caused by O_2 admission and scrambling of oxygen in CO and O_2 occurred (4, 5, 22, 37). Haruta *et al.* claimed that CO molecules and O atoms (dissociated from O_2) are adsorbed in the neighborhood of each other on a Au particle with electronic interaction favorable for CO oxidation, forming a OC–Au–O intermediate (4, 5, 22, 37). As for the Au/Ti(OH)$_4^*$ catalyst O_2 is not directly bound to the Au particles in agreement with Fukushima *et al.* (47) who observed no detectable oxygen adsorption on Au particles on SiO_2, MgO, and Al_2O_3 below 443 K. No measurable adsorbed oxygen was detected on Au(111) after exposure to O_2 at high pressures and temperatures (48, 49).

The intensity of the two ν_{CO} peaks at 2136 and $2119\ cm^{-1}$ for CO adsorbed on Au particles in the steady-state CO oxidation with O_2 was smaller than that under identical CO pressure without O_2 as shown in Fig. 13. The reduced peak intensity during the steady-state CO oxidation on Au/Ti(OH)$_4^*$ can be explained as a result of the balance between CO adsorption on the Au particles and the successive reaction with O_2^- adsorbed on the oxide surface at the boundary. Both bands at 2136 and $2119\ cm^{-1}$ reacted with oxygen and eventually disappeared at room temperature. The band at $2136\ cm^{-1}$ remained after 2 min of evacuation, to which O_2 was admitted, leading to CO oxidation. The peak intensity at $2188\ cm^{-1}$ for CO adsorbed on Ti^{4+} in the presence of O_2 was almost the same as that in the absence of O_2 at the identical CO pressure, which implies that the CO molecules on Ti^{4+} sites are much less reactive to oxygen. This was also found with Au/Fe(OH)$_3^*$, which showed a remarkably high activity for the catalytic CO oxidation. The CO molecules adsorbed on Fe^{3+} sites of the oxide surface did not react with O_2 (50). Thus it is suggested that only CO molecules adsorbed on Au metallic particles in Au/Ti(OH)$_4^*$ contribute to the catalytic CO oxidation with O_2.

It is to be noted that CO does not adsorb on Ti^{4+} ions on TiO_2^* as shown in Fig. 12 (curve g). The Au particles markedly influenced the morphology of the Ti oxide surface and provided coordinatively unsaturated Ti^{4+} ions available

for CO adsorption besides oxygen vacancies for O_2 adsorption. It is also to be noted that annealing of Au/Ti(OH)$_4^*$ did not have any significant effect on the Au particle surface in that there was no change in CO adsorption, as shown in Fig. 12 (curve h), while the annealing decreased the amount of adsorbed O_2 probably due to a decrease in the amount of oxygen vacancies.

The mechanism for the catalytic CO oxidation on supported Au catalysts has been studied by several groups (4, 5, 9, 19, 21–24, 37, 51, 52). Au(I) and Au(0) sites as well as the boundary between Au particle and support have been proposed as reaction sites. Minico *et al.* suggested by FT-IR study that Au(I) is more active but less stable than Au(0) in a noncalcined Au/Fe_2O_3 catalyst prepared by a coprecipitation method (19). Au(I) species may not work as a stable, active catalyst under the steady-state reaction conditions with long life. Haruta *et al.* (21), Wagner *et al.* (10), and Epling *et al.* (52) have observed oxidized Au species in coprecipitated Au/Fe_2O_3 and Au/Co_3O_4 catalysts by XPS and Mössbauer spectroscopies, but they have found no direct correlation between the content of oxidized Au species and the performance of the catalysts. To explain the high activity of Au catalysts prepared by coprecipitation and deposition–precipitation methods, a scheme that involves catalysis on the boundary of small Au particles and support was proposed by Haruta *et al.* (4, 5, 21). The proposed mechanism involves reversible adsorption of CO on the surface and perimeter of Au particles and irreversible adsorption of oxygen at the perimeter interface to form a OC–Au–O intermediate, which is converted to CO_2 (4). The hypothesis was supported by a FT-IR study performed by Boccuzzi *et al.* who studied the CO oxidation and oxygen scrambling on Au/TiO_2 and Au/ZnO (22, 23, 37). They thought that gold sites could adsorb both CO and oxygen atoms at the same time judging from the frequency shift of adsorbed CO bands in the presence of O_2 and the occurrence of oxygen scrambling between CO and $^{36}O_2$. They also found that the bidentate carbonate species produced in the reaction of CO + $^{32}O_2$ is identical to that produced in the reaction of CO + $^{36}O_2$. Based on these results, they proposed that CO is oxidized to CO_2 through two independent pathways: one is the rapid reaction between CO and atomic oxygen, both adsorbing on the same Au particle surface, and the other is the slower decomposition of the carbonates, which are formed by interaction of adsorbed CO with surface lattice oxygen atoms of the support. Vannice *et al.* (9, 51) suggested a two-site Langmuir–Hinshelwood model where CO adsorbed on Au particles reacts with oxygen molecules at the Au particle–TiO_2 boundary on the basis of the kinetic and DRIFTS studies. They excluded the possibility of dissociative adsorption of O_2 from calculation of the thermodynamic parameters of adsorption. A completely different mechanism for CO oxidation on a coprecipitated Au/ZrO_2 catalyst has been proposed by Knell *et al.* (24). Adsorbed CO reacts first with surface hydroxyl groups to produce formates. Then the formates are oxidized to carbonates by surface oxygen atoms. A catalytic cycle is completed by CO_2 desorption and excess oxygen results in deactivation of the catalyst. Such a route may be minor on the catalysts pretreated in dry air (22), but it can probably operate in the presence of moisture. A positive effect of moisture on CO oxidation on a coprecipitated Au catalyst with Au loadings below 0.4 wt% was reported by Haruta *et al.* (5), whereas the presence of water vapor significantly suppressed the reaction on the present Au/Ti(OH)$_4^*$ catalyst. Our results demonstrate that low-temperature CO oxidation on the Au/Ti(OH)$_4^*$ catalyst involves reversible CO adsorption on the Au particle surface, O_2 adsorption on oxygen vacancies on the Ti oxide support adjacent to the Au particles forming O_2^-, and subsequent reaction between CO and O_2^-. The reaction orders with respect to CO and O_2 pressures on the Au/Ti(OH)$_4^*$ catalyst were 0.25 and 0.41, respectively, which can be described with the reaction (Langmuir–Hinshelwood model) between adsorbed CO and O_2^- species as the rate-determining step. The activation energy for the catalytic CO oxidation was calculated to be 24 kJ mol^{-1}, which falls in the range 17–29 kJ mol^{-1} reported by Vannice *et al.* (9, 51). The present conclusion does not deny the reaction of CO and atomic oxygen, which is known as a ready reaction. If atomic oxygen were produced by dissociation of O_2 on the Au/Ti(OH)$_4^*$ catalyst, the catalytic CO oxidation would also have proceeded via the atomic oxygen. It seems that dissociation of O_2 molecules is slow on the Au/Ti(OH)$_4^*$ surface, but adsorbed O_2^- readily reacts with CO to form CO_2 and active oxygen atom which rapidly reacts with CO to form another CO_2. Mechanism [3] may be divided into two successive oxidation reactions ($CO\,(a) + O_2^* \rightarrow CO_2 + O^*$, $O^* + CO\,(a) \rightarrow CO_2$), where the first step is a rate-determining step for catalytic CO oxidation on Au/Ti(OH)$_4^*$. The mechanism for catalytic CO oxidation on a remarkably active Au/Fe(OH)$_3^*$ catalyst will be discussed in a following paper (50).

5. CONCLUSIONS

1. The Au/Ti(OH)$_4^*$ catalyst was inactive in oxygen isotope exchange between gaseous oxygen and lattice oxygen atoms and between oxygen molecules at room temperature.

2. The Au/Ti(OH)$_4^*$ catalyst was also inactive in oxygen exchange between CO and lattice oxygen atoms and between CO and gaseous oxygen.

3. The lattice oxygen atoms of the Au/Ti(OH)$_4^*$ catalyst were active only in oxygen exchange with CO_2.

4. CO was not oxidized with lattice oxygen atoms on Au/Ti(OH)$_4^*$, but oxidized with adsorbed molecular oxygen at room temperature.

5. CO molecules reversibly adsorbed on both Au particles and Ti^{4+} sites. Only the CO molecules adsorbed on Au contributed to the catalytic CO oxidation.

6. O_2 adsorbed on oxygen vacancies at the Ti oxide surface in the form of superoxide O_2^- with an angular arrangement ($g_1 = 2.020$, $g_2 = 2.010$, and $g_3 = 2.005$).

7. The CO molecules on Au particle surfaces and the O_2^- species on oxygen vacancies adjacent to the Au particles were responsible for the catalytic CO oxidation on the $Au/Ti(OH)_4^*$ catalyst at room temperature.

8. Annealing of $Au/Ti(OH)_4^*$ significantly suppressed the catalytic activity due to a decrease in the amount of oxygen adsorption.

ACKNOWLEDGMENT

This work has been supported by CREST (Core Research for Evolutional Science and Technology) of Japan Science and Technology Corporation (JST).

REFERENCES

1. Hammer, B., and Norskov, J. K., *Nature* **238**, 376 (1995).
2. Huber, H., McIntosh, D., and Ozin, G. A., *Inorg. Chem*. **16**, 975 (1977).
3. Haruta, M., Yamada, N., Kobayashi, T., and Iijima, S., *J. Catal.* **115**, 301 (1989).
4. Haruta, M., *Catal. Today* **36**, 153 (1997).
5. Haruta, M., *Catal. Surv. Jpn*. **1**, 61 (1997).
6. Hutchings, G. J., Siddigui, M. R. H., Burrows, A., Kiely, C. J., and Whyman, R., *J. Chem. Soc. Faraday Trans.* **93**, 187 (1997).
7. Hoflund, G. B., Gardner, S. D., Schryer, D. R., Upchurch, B. T., and Kielin, E. J., *Appl. Catal. B: Environ*. **6**, 117 (1995).
8. Baiker, A., Maciejewski, M., Tagliaferri, S., and Hug. P., *J. Catal.* **151**, 407 (1995).
9. Bollinger, M. A., and Vannice, M. A., *Appl. Catal. B: Environ.* **8**, 417 (1996).
10. Wagner, F. E., Galvagno, S., Milone, C., Visco, A. M., Stievano, L., and Calogero, S., *J. Chem. Soc. Faraday Trans.* **93**, 3403 (1997).
11. Yuan, Y., Asakura, K., Wan, H., Tsai, K., and Iwasawa, Y., *Chem. Lett.* 755 (1996).
12. Yuan, Y., Kozlova, A. P., Asakura, K., Wan, H., Tsai, K., and Iwasawa, Y., *J. Catal.* **170**, 191 (1997).
13. Kozlova, A. P., Sugiyama, S., Kozlov, A. I., Asakura, K., and Iwasawa, Y., *J. Catal.* **176**, 426 (1998).
14. Kozlov, A. I., Kozlova, A. P., Liu, H. C., and Iwasawa, Y., *Appl. Catal. A: General* **182**, 9 (1999).
15. Mathieson, T. J., Langdon, A. G., Milestone, N. B., and Nicholson, B. K., *J. Chem. Soc. Chem. Commun*. 371 (1998).
16. Yuan. Y., Asakura, K., Kozlova, A. P., Wan, H., Tsai, K., and Iwasawa, Y., *Catal. Today* **44**, 333 (1998).
17. Okumura, M., Tanaka, A., Ueda, M., and Haruta, M., *Solid State Ionics* **95**, 143 (1997).
18. Haruta, M., *Stud. Surf. Sci. Catal.* **110**, 123 (1997).
19. Minico, S., Scire, S., Crisafulli, C., Visco, A. M., and Galvagno, S., *Catal. Lett.* **47**, 273 (1997).
20. Liu, W., and Flytzani-Stephanopoulos, M. J., *J. Catal.* **153**, 317 (1995).
21. Haruta, M., Tsubota, S., Kobayashi, T., Kageyama, H., Genet, M. J., and Delmon, B., *J. Catal.* **144**, 175 (1993).
22. Boccuzzi, F., Chiorino, A., Tsubota, S., and Haruta, M., *J. Phys. Chem*. **100**, 3625 (1996).
23. Boccuzzi, F., Guglielminotti, E., Pinna, F., and Strukul, G., *Surf. Sci.* **377–379**, 728 (1997).
24. Knell, A., Barnickel, P., Baiker, A., and Wokaun, A., *J. Catal.* **137**, 306 (1992).
25. Na, B. K., Walters, A. B., and Vannice, M. A., *J. Catal.* **140**, 585 (1993).
26. Lunsford, J. H., and Jayne, J. P., *J. Chem. Phys.* **44**, 1492 (1966).
27. Kokes, R. J., *J. Phys. Chem*. **66**, 99 (1962).
28. Naccache, C., Meriaudeau, P., and Che, M., *Trans. Faraday Soc.* **67**, 506 (1971).
29. Cornaz, P. F., van Hooff, J. H. C., Plujim, F. J., and Schuit, G. C. A., *Discuss. Faraday Soc.* **41**, 290 (1966).
30. van Hooff, J. H. C., *J. Catal.* **11**, 277 (1968).
31. Shvets, V. A., and Kazansky, V. B., *J. Catal.* **25**, 123 (1972).
32. Che, M., and Tench, A. J., *Adv. Catal.* **32**, 1 (1983).
33. Soria, J., Coronado, J. M., and Conesa, J. C., *J. Chem. Soc. Faraday Trans.* **92**, 1619 (1996).
34. Martinez-Arias, A., Coronado, J. M., Cataluna, R., Conesa, J. C., and Soria, J., *J. Phys. Chem*. **102**, 4357 (1998).
35. Meriaudeau, P., and Vedrine, J. C., *J. Chem. Soc., Faraday Trans. II* **72**, 472 (1976).
36. Little, L. H., Kiselev, A. V., and Lygin, V. I., "Infrared Spectra of Adsorbed Species," p. 18, Academic Press, New York, 1966.
37. Boccuzzi, F., Chiorino, A., Tsubota, S., and Haruta, M., *Catal. Lett.* **29**, 225 (1994).
38. Hashimoto, K., Fukuhara, K., Fujiwara, Y., Kominami, H., Mishima, H., and Kera, Y., *Appl. Catal. A: General* **165**, 451 (1997).
39. Iwamoto, M., Yoda, Y., Yamazoe, N., and Selyama, T., *J. Phys. Chem*. **82**, 2564 (1978).
40. Soria, J., Martinez-Arias, A., Coronado, J. M., and Conesa, J. C., *Colloids Surf. A* **115**, 215 (1996).
41. Morazzoni, F., Scotti, R., and Volonte, S., *J. Chem. Soc. Faraday Trans.* **86**, 1587 (1990).
42. France, J., and Hollins, P., *J. Electron Spectrosc. Relat. Phenom*. **64–65**, 251 (1993).
43. Morterra, C., *J. Chem. Soc. Faraday Trans. I* **84**, 1617 (1988).
44. Salama, T. M., Shido, T., Ohnishi, R., and Ichikawa, M., *J. Phys. Chem*. **100**, 3688 (1996).
45. Guillemot, D., Borovkov, V. Yu., Polisset-Thfoin, M., and Fraissard, J., *J. Chem. Soc. Faraday Trans.* **93**, 3587 (1997).
46. Kozlova, A. P., Asakura, K., Kozlov, A. I., Sugiyama, S., Matsui, Y., and Iwasawa, Y., *J. Catal.* **181**, 37 (1999).
47. Fukushima, T., Galvagno, S., and Parravano, G., *J. Catal.* **57**, 177 (1979).
48. Pireaux, J. J., Chtaib, M., Delrue, J. P., Thiry, P. A., Liehr, M., and Caudano, R., *Surf. Sci.* **141**, 211 (1984).
49. Sault, A. G., Madix, R. J., and Campbell, C. T., *Surf. Sci.* **169**, 347 (1986).
50. Liu, H., Kozlov, A. I., Kozlova, A. P., Shido, T., Asakura, K., and Iwasawa, Y., *Phys. Chem. Chem. Phys.*, in press.
51. Lin, S. D., Bolinger, M., and Vannice, M. A., *Catal. Lett.* **17**, 245 (1993).
52. Epling, W. S., Hoflund, G. B., Weaver, J. F., Tsubota, S., and Haruta, M., *J. Phys. Chem*. **100**, 9929 (1996).